RESEARCH ARTICLE

Sampling volume assessment for wearable multimodal optical diagnostic device

Elena V. Zharkikh [ID] | **Viktor V. Dremin** [ID] | **Andrey V. Dunaev** [ID]

Research & Development Center of Biomedical Photonics, Orel State University, Orel, Russia

Correspondence
Elena Zharkikh, Research & Development Center of Biomedical Photonics, Orel State University, 95, Komsomolskaya Str., Orel 302026, Russia.
Email: ev.zharkikh@gmail.com

Funding information
Russian Science Foundation, Grant/Award Number: 23-25-00522

Abstract

The process and results of numerical Monte Carlo simulation of optical radiation propagation in laser Doppler flowmetry (LDF) and fluorescence spectroscopy (FS) channels of a wearable diagnostic multimodal device are described in this paper. To achieve the goal, a multilayer skin model with different parameters of blood and melanin content and different distances between sources and radiation receivers was designed. The changes in the sampling (diagnostic) volume depending on the anatomical features of the biological tissues, as well as on the technical parameters of the device were shown. Depending on the scattering media optical properties and the source-detector configuration of the device, the diagnostic volume can range from 2 to 7 mm^3. The obtained results allow the formation of specialized medical and technical requirements for wearable multimodal devices implementing LDF and FS channels.
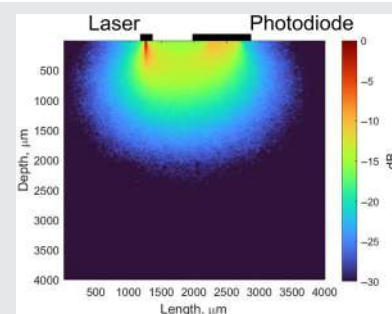
KEYWORDS
fluorescence spectroscopy, laser doppler flowmetry, Monte Carlo simulations, optical noninvasive diagnostics, optical properties, wearable device

1 | INTRODUCTION

Microcirculatory-tissue systems are the object of study for many contemporary optical noninvasive diagnostic methods [1, 2]. The microcirculatory bed is a complexly organized system that carries out the exchange between blood and tissues necessary to ensure cellular metabolism and removal of metabolic products. And consequently, the microcirculatory system is the first link that is involved in the pathological process in various extreme situations. For example, disturbances in the circulatory system occur in such common diseases as diabetes mellitus [3, 4], hypertension [5, 6], and coronavirus infection [7].

Laser Doppler flowmetry (LDF) is a noninvasive method of assessing the state of the microcirculatory blood flow. This method analyses the back-reflected component of optical radiation from biological tissue to measure microcirculatory blood flow parameters. When emitted light is scattered by a moving object, the frequency of the probing radiation changes according to the Doppler effect, with other part of the flux being scattered from stationary particles the frequency of the radiation respectively remains unchanged [8, 9]. In studies conducted on the human skin in vivo when both parts of the photon flux are detected in the photodetector, a photocurrent is generated, the spectral power density of which
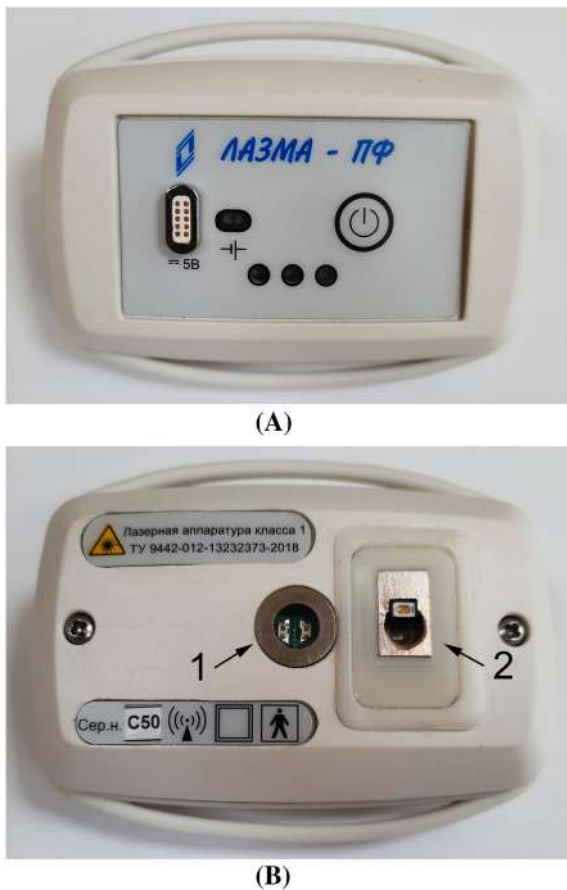
FIGURE 1 (A) Appearance of wearable devices implementing LDF and FS diagnostic channels and (B) the back panel featuring LDF (1) and FS (2) channels. LDF, laser Doppler flowmetry; FS, fluorescence spectroscopy.

is proportional to the velocity of the red blood cells in the perfused tissue [10]. The result of LDF measurements is formed as an index of microcirculation (perfusion) measured in perfusion (arbitrary) units. The method was first introduced over 40 years ago and has undergone continuous development since [11].

Fluorescence spectroscopy (FS) is another optical noninvasive diagnostic technique widely used in clinical research. This method is based on excitation of fluorescence of endogenous and exogenous fluorophores of biological tissues and recording the emission in the visible region of the spectrum. This method is highly sensitive and allows noninvasive diagnosis of oxidative metabolism of biological tissues [12, 13].

To date, many devices have been developed that implement LDF and FS methods together according to a multimodal approach or separately, and they are widely used in scientific research [2]. Unfortunately, the methodological and instrumental complexity of their implementation, including the mass-size parameters of devices and the usage of fiber-optic probes to transmit optical

radiation to the skin, hinder a wider implementation of these methods in clinical practice. Due to the high requirements for probing and receiving parts of LDF devices (radiation sources in the form of single-mode lasers, radiation receivers, delivery, and reception systems of radiation from biological tissues), there have so far been very few studies on the possibility of miniaturization and development of wearable devices [14, 15], allowing to significantly increase the convenience of their application and, consequently, expand their field of implementation in clinical practice. However, due to the development of miniaturized laser sources (first of all, vertical-cavity surface-emitting lasers [VCSEL]), a significant breakthrough has been made in this area recently—wearable devices "LAZMA PF" (LAZMA Ltd, Russia; in EU/UK this device made by Aston Medical Technology Ltd., UK as "FED-1b") implementing LDF, FS, cutaneous thermometry, and accelerometry channels, operating directly without optical fiber and transmitting measurement data to a PC using Bluetooth or Wi-Fi protocols [16, 17]. The appearance of the wearable multimodal devices implementing LDF and FS methods is shown in Figure 1.

These devices are gradually finding their application in medical practice, especially in the diagnosis of complications associated with diabetes mellitus [18, 19], hypertension [20], have been tested in the assessment of smoking status [21], effectiveness of drug therapy for microcirculatory disorders [22], in assessing the influence of the body position on microcirculation parameters [23], assessment of blood microcirculation changes after COVID-19 [24] and under the microgravity conditions during the Space flight [17, 25]. However, for their wider introduction into clinical practice, additional research is required, and first of all, it is necessary to substantiate specialized medical and technical requirements of metrological nature [26], taking into account the peculiarities of design of these wearable multimodal devices.

As is known, human skin is an optically heterogeneous scattering medium [27], and the values of signals recorded from it using optical noninvasive diagnostic methods strongly depend on its optical properties. The technical characteristics of the diagnostic device, such as the size of the source and detector, the distance between them, numerical aperture, and so on, also have a significant influence on the recorded signal. In this regard, an important task is the theoretical evaluation of the influence of skin optical properties on the formation of the recorded signal. Thus, this work was aimed at studying the features of optical radiation propagation of LDF and FS channels of a wearable multimodal diagnostic device in biological tissues based on Monte Carlo (MC) simulation method.
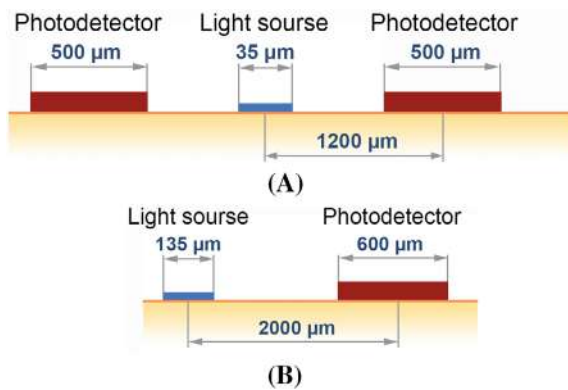
FIGURE 2 Geometric dimensions and arrangement of light sources and photodetectors in the (A) LDF and (B) FS channels of the wearable multimodal diagnostic device. LDF, laser Doppler flowmetry; FS, fluorescence spectroscopy.

2 | MATERIALS AND METHODS

2.1 | MC simulation

A model of optical radiation propagation in the skin has been proposed to analyze sampling volume in the LDF and FS channels of a wearable multimodal diagnostic device. The skin is the largest organ of the human body in terms of area and has a complex structure [28]. In this paper, human skin model was represented as a three-dimensional semi-infinite medium divided into several layers with different optical properties.

In order to simulate the sampling volume, the geometrical features of the emitting and recording parts of the LDF and FS channels of a wearable multimodal device (size and profile of the light source beam, size and position of the light sources and detectors, and intercenter distance between them) were taken into account. In the wearable devices for which the simulations were performed, the LDF channel is implemented using a VCSEL emitting at a wavelength of 850 nm with a continuous power of less than 1 mW (Philips, the Netherlands). The FS channel is designed to use 365-nm light-emitting diode as a source for fluorescence excitation with the average output power of 0.35 mW. The geometric dimensions and arrangement of the sources and detectors (the distance between them—the so-called "measurement base," r [29]) of the optical emission of the LDF (Figure 2A) and FS (Figure 2B) channels of the wearable multimodal device are shown in Figure 2.

In this study, a stochastic MC method was used to simulate the propagation of optical radiation in biological tissue. The MC method provides a flexible and accurate solution to the problem of light transport in turbid media with a complex structure, which has made it a popular tool

for simulating optical radiation propagation in biological tissues. In the general MC simulation procedure, light transport in tissues is simulated by tracking the random steps that each photon packet takes as it travels in a tissue model. An online object-oriented MC computational tool has been used to simulate the sampling volume of the LDF channel [30–32]. This approach allows to describe photons and tissue structural components as objects that interact with each other. Thus, a photon propagates through a medium (or layer of a medium) and interacts with its components, such as cells, blood vessels, collagen fibers, and so on. This representation of the medium by objects allows the development of realistic tissue models that represent three-dimensional spatial variations in biological structure. The simulation takes into account the detector depth sensitivity (also known as diagnostic volume or sampling volume). This model does not take into account the Doppler frequency shift nor secondary fluorescence emission. We assume that the results obtained represent the maximum depth value that can be reached by irradiation skin tissue with wavelengths of 850 and 365 nm, thus allowing to access the diagnostic volume for these technologies. The sampling volume in this work was calculated until the amount of detected photons reached the value of 10^6.

2.2 | Human skin model

A seven-layer skin tissue model was used to simulate the sampling volume and the depth of penetration of the probe radiation for the LDF channel, which was originally proposed in an earlier article [33]. This model takes into account the absorption and scattering properties of the tissues. The absorption coefficients μ_a of the skin layers were calculated taking into account blood concentration, oxygen saturation, water and fat content, hematocrit, and melanin fraction. The scattering coefficient μ_s of a particular layer can be represented by a combination of Mie/Rayleigh theories [34]. Values of scattering coefficients for different skin layers have been obtained from a number of sources [27, 35–38]. The anisotropy coefficient g was calculated by analogy with the absorption coefficient calculation. Skin and blood anisotropy coefficients were used for the calculations [39, 40].

For the present study, the model was adapted to account for the different blood flow and different melanin content in the tissue. For the LDF channel analysis, blood concentration values for each skin layer were varied in 20% increments according to the following formula:

$$C_{\text{blood}}^{\text{LDF}} = C_{\text{blood}}^{i} \cdot k_{\text{LDF}}, \tag{1}$$

Layer	Blood volume fraction, %	μ_s, mm^{-1}	g	n	d, µm
Stratum corneum	0	25.28	0.87	1.55	20
Living epidermis	0	17.62		1.43	80
Papillary dermis	5	10.89		1.38	100
Upper blood net dermis	20				80
Reticular dermis	4				1620
Deep blood net dermis	10				200
Subcutaneous tissue	7	9.85		1.44	5900

TABLE 1 Basic characteristics of the skin model under the study for the wavelength of 850 nm.

TABLE 2 Absorption coefficient at 850 nm for different variations in blood and melanin content.

Layer	μ_a, mm^{-1}									
	Blood content variation (k_{LDF})									
	0.2	0.4	0.6	0.8	1.0	1.2	1.4	1.6	1.8	2.0
Stratum corneum	0.03									
Living epidermis	0.14									
Papillary dermis	0.04	0.04	0.05	0.05	0.05	0.06	0.06	0.07	0.07	0.08
Upper blood net dermis	0.06	0.08	0.10	0.12	0.14	0.16	0.18	0.20	0.22	0.24
Reticular dermis	0.04	0.05	0.05	0.06	0.06	0.07	0.07	0.08	0.08	0.09
Deep blood net dermis	0.05	0.06	0.07	0.08	0.09	0.10	0.11	0.12	0.13	0.14
Subcutaneous tissue	0.03	0.04	0.05	0.06	0.06	0.06	0.08	0.09	0.09	0.10
	Melanin content variation ($C_{melanin}^{LDF}$)									
	0.01	0.05	0.10	0.15	0.20	0.25	0.30	0.35	0.40	
Living epidermis	0.14	0.57	1.11	1.65	2.20	2.74	3.28	3.82	4.36	

where C_{blood}^i is the baseline blood volume fraction of each particular skin layer and $k_{LDF} = 0.2, 0.4, ..., 2$.

Next, to account for the influence of the melanin content in the skin on the penetration depth of the probing radiation, the sampling volume was estimated with normal blood content $k_{LDF} = 1$ and the melanin content of the epidermis varying between $C_{melanin}^{LDF} = 0.01, 0.05, 0.1, 0.15, ..., 0.4$ [41, 42].

Tables 1 and 2 show basic optical properties at the wavelength of 850 nm of the seven-layer skin model taken into account in this study, as well as the variations in the absorption coefficient caused by different blood and melanin content.

Finally, we evaluated the influence of the measurement base (r) in the LDF channel on the penetration depth of the probing radiation. It has been demonstrated earlier that source-detector separation greatly affects the sampling depth in optical diagnostic methods (in particular, in diffuse reflectance spectroscopy) [43, 44]. For the LDF channel, r varied in the range from 500 to 1200 µm with the increment of 100 µm. The influence of the blood volume fraction and melanin content

in the skin on the depth of signal propagation at different r values was also analyzed.

For the FS channel, all the same operations were done as for the LDF. However, due to the high-optical radiation absorption by the skin at the used wavelength (365 nm), a three-layer skin model was used to facilitate the simulation, including the *stratum corneum*, epidermis, and the upper part of the dermis. Here, in order to evaluate the effect of different blood volume on the penetration depth of the probing radiation, the Formula (1) was adapted as follows:

$$C_{blood}^{FS} = C_{blood}^i \cdot k_{FS}, \qquad (2)$$

where $k_{FS} = 0.25, 0.375, ..., 1$.

The effect of melanin content was evaluated separately, varying its content in the epidermis between 1%, 3%, 5%, and 10% ($C_{melanin}^{FS} = 0.01, 0.03, 0.05, 0.1$) while the blood concentration was lowest in this simulation ($k_{FS} = 0.25$). Finally, the measurement base for the FS channel varied in the range from 500 to 2000 µm with the

TABLE 3 Basic characteristics of the used skin model for the wavelength 365 nm.

Layer	Blood volume fraction, %	μ_s, mm^{-1}	g	n	d, µm
Stratum corneum	0	77.48	0.73	1.55	20
Living epidermis	0	61.37		1.47	80
Dermis	6	43.76		1.40	1800

TABLE 4 Absorption coefficient at 365 nm for different variations in blood and melanin content.

Layer	μ_a, mm^{-1}						
	Blood content variation (k_{FS})						
	0.25	0.375	0.50	0.625	0.75	0.875	1.0
Stratum corneum	0.36						
Living epidermis	2.36						
Dermis	0.42	0.57	0.72	0.87	1.02	1.17	1.32
	Melanin content variation ($C_{melanin}^{LDF}$)						
	0.01	0.03		0.05		0.10	
Living epidermis	0.14	0.57		1.11		1.65	

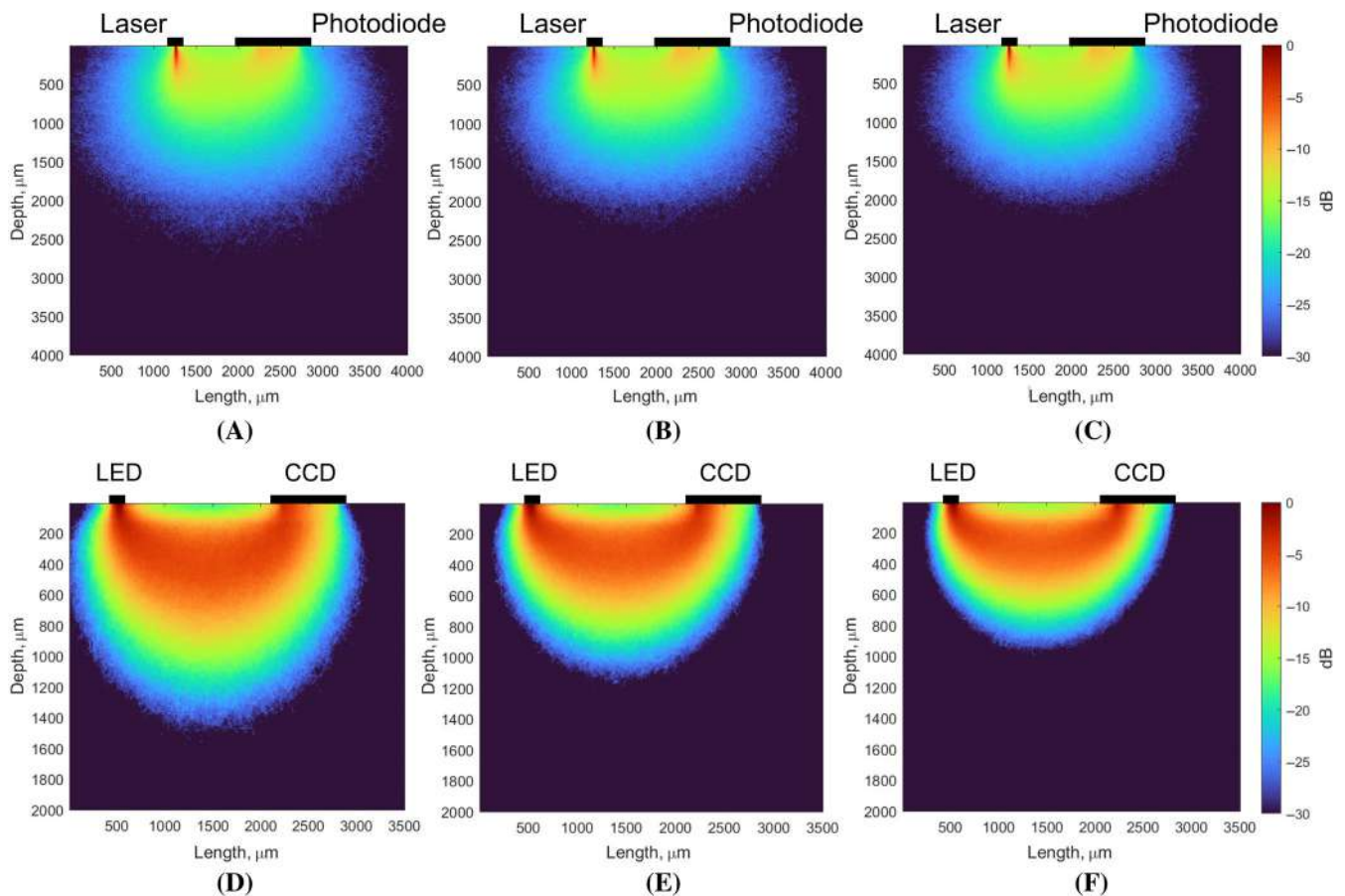**FIGURE 3** Sampling volume for the back-scattered diffuse reflectance probe, schematically presented in Figure 2: (A) for $k_{LDF} = 0.2$, (B) for $k_{LDF} = 1.0$, (C) for $k_{LDF} = 2.0$, (D) for $k_{FS} = 0.25$, (E) $k_{FS} = 0.625$, and (F) $k_{FS} = 1.0$. (A–C) Simulation results for the LDF channel; (D–E) simulation results for the FS channel. LDF, laser Doppler flowmetry; FS, fluorescence spectroscopy.
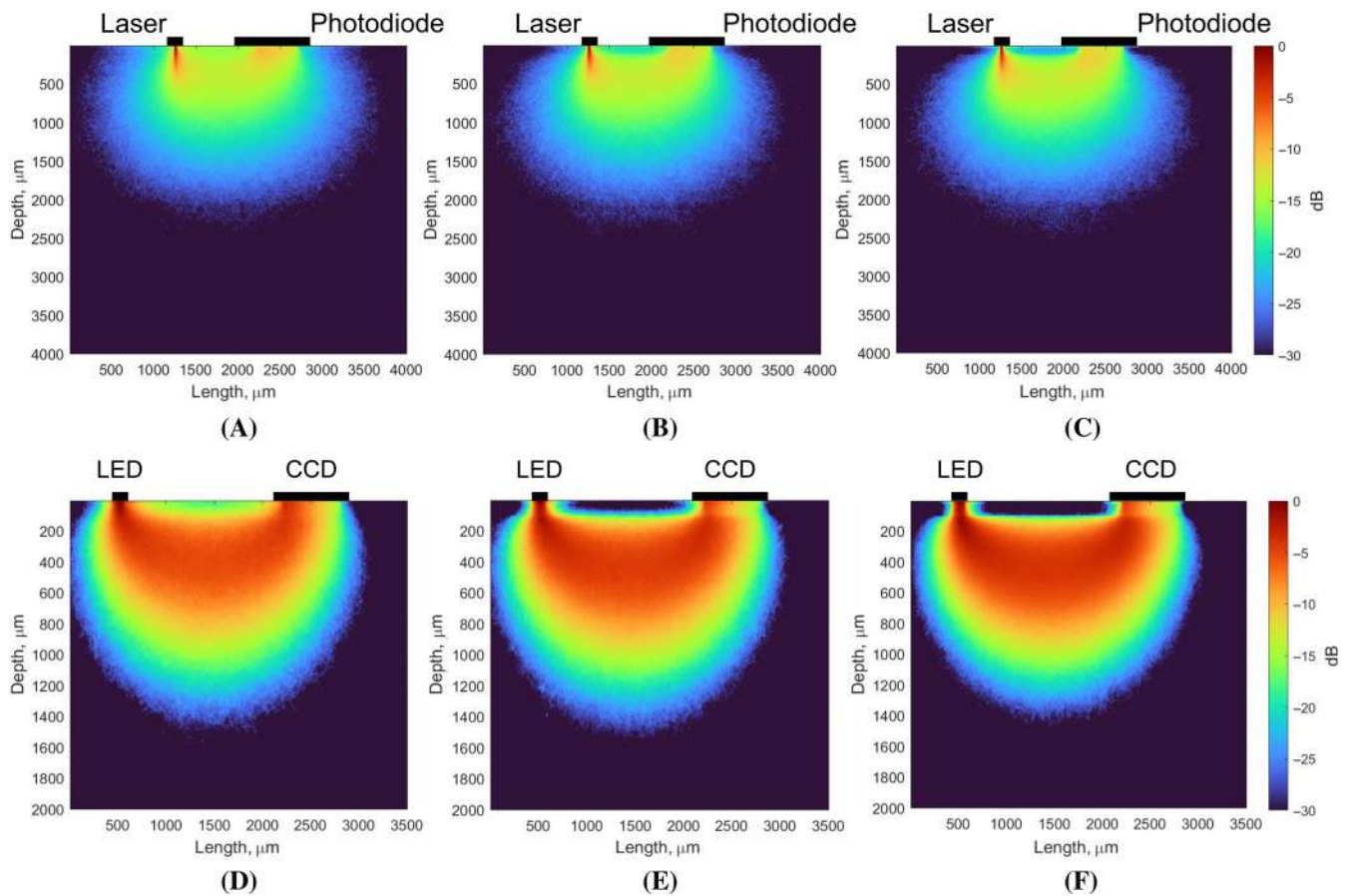
FIGURE 4 Sampling volume for the back-scattered diffuse reflectance probe, schematically presented in Figure 2: (A) for $C_{melanin}^{LDF} = 0.01$, (B) $C_{melanin}^{LDF} = 0.2$, (C) $C_{melanin}^{LDF} = 0.4$, (D) $C_{melanin}^{FS} = 0.01$, (E) $C_{melanin}^{FS} = 0.05$, and (F) $C_{melanin}^{FS} = 0.1$. (A–C) Simulation results for the LDF channel; (D–E) simulation results for the FS channel. LDF, laser Doppler flowmetry; FS, fluorescence spectroscopy.

increment of 100 μm. The main optical characteristics of the studied skin model for 365 nm and the variation in absorbance at this wavelength for different blood and melanin content are shown in Tables 3 and 4.

3 | RESULTS AND DISCUSSION

Figure 3 demonstrates the results of a MC simulation of the optical radiation propagation in the LDF (A–C) and FS (D–F) channels of a wearable diagnostic device for the human skin with different blood content. For the calculations shown in this figure, $C_{melanin}^{LDF}$ and $C_{melanin}^{FS}$ values were assumed to be 0.01, the r value for the LDF channel is 1200 μm, for the FS channel is 2000 μm. In order to adequately assess from which skin layers the diagnostically valuable signal is coming, the depth of light penetration was calculated at the level of 10^{-3} of the incident light intensity [45]. This value was chosen because it represents the minimum sensitivity of most commercially available photodetectors. In addition, the value of the volume of biological tissue subjected to diagnosis was

calculated. The volume was calculated from the registered optical scattering diagrams as the value of the volume of the ellipsoid described by the zero coordinate and the line where signal attenuates by more than three orders of magnitude.

Simulation results showed that in the current modification of the wearable LDF device the probing radiation penetrates to a depth of more than 2 mm, reaching deep vascular plexuses. An increase in blood content in the skin leads to a decrease in probing depth, so it can be assumed that in more blood-filled areas of the skin, diagnostic information will come from shallower tissue layers. Diagnostic volume of LDF channel in this case is 6–7 mm^3.

A similar situation was observed for the FS channel (Figure 3D,E), with a calculated penetration depth of 1 mm for probing radiation under normal conditions. Diagnostic volume of FS channel in this case is 2–2.5 mm^3. It should also be noted that in this simulation, with k_{FS} set to 1.2, such a source-detector configuration did not allow successful sampling volume evaluation due to a high light absorption. Under the specified
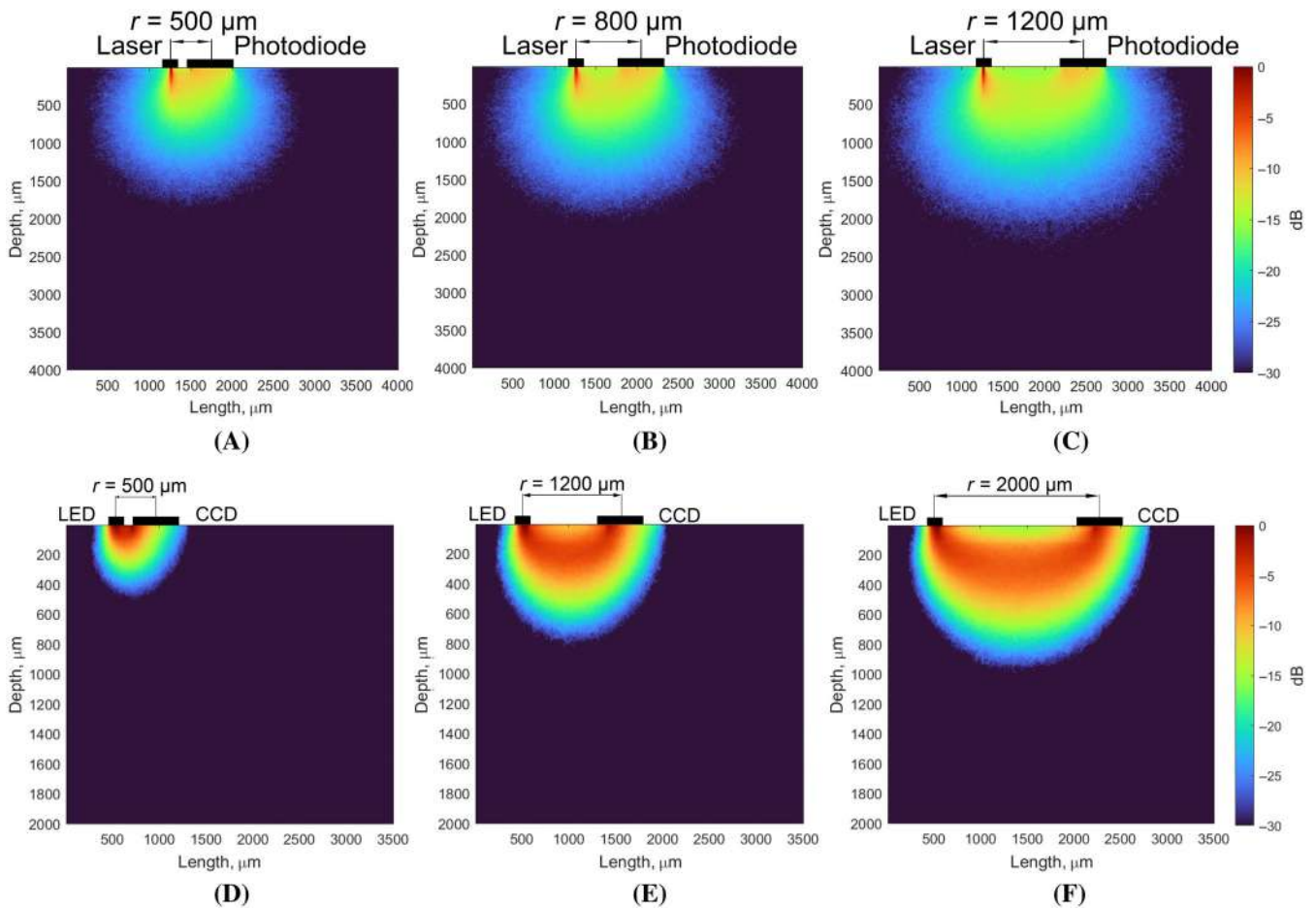
FIGURE 5 Sampling volume for the back-scattered diffuse reflectance probes, schematically presented in Figure 2: (A) for $r = 500$, (B) for $r = 800$, (C) for $r = 1200$ μm for the LDF channel, and (D) for $r = 500$, (E) for $r = 1200$, (F) for $r = 2000$ μm for the FS channel. (A–C) Simulation results for the LDF channel; (D–E) simulation results for the FS channel. LDF, laser Doppler flowmetry; FS, fluorescence spectroscopy.

boundary conditions ($k_{FS} = 1$ and $r = 2000$ μm) more than 4.5 billion photons had to be generated to register only 10^6 of photons on the photodetector (see Supplementary Figure 1). It can be assumed that by decreasing the value of r it is possible to register a signal in tissues with higher blood filling from greater depths.

Figure 4 shows the results of a MC simulation of the optical radiation propagation in the LDF (A–C) and FS (D–F) channels of a wearable diagnostic device for the human skin with different melanin content. For the calculations shown in this figure, k_{LDF} and k_{FS} values were assumed to be equal to 1 and 0.25, respectively, the r value for the LDF channel is 1200 μm and for the FS channel is 2000 μm.

Figure 4 shows that with the given device design parameters ($r = 2000$ μm), melanin content has no significant effect on the sampling volume both in the LDF and FS channels, but the skin richer in melanin is characterized by less scattering of optical radiation in the subsurface layers. In the FS channel, for higher melanin

content in the epidermis, actually the main signal comes only from the dermis layers, which is due to the absorption of UV radiation by melanin. Thus, it can be said that with a high melanin content in the epidermis, there is minimal diffuse light scattering due to high absorption. For the values of $C_{melanin}^{FS} > 0.1$, the simulation was not performed due to the high absorption and the extensive amount of time required to carry out such simulation (for more information, see Supplementary Figure 2). Due to the large source-receiver separation in this diagnostic channel photons need to propagate over a long distance before being absorbed, that makes MC simulation very computationally extensive [46].

Our work further investigated how changing the measurement base affects the value of the sampling volume when probing biological tissue with 850 and 365 nm light. For this purpose, the simulation varied the distance between the light source and photodetector from 500 to 1200 μm with increments of 100 μm for the LDF channel. Similar simulations have been done for the FS channel
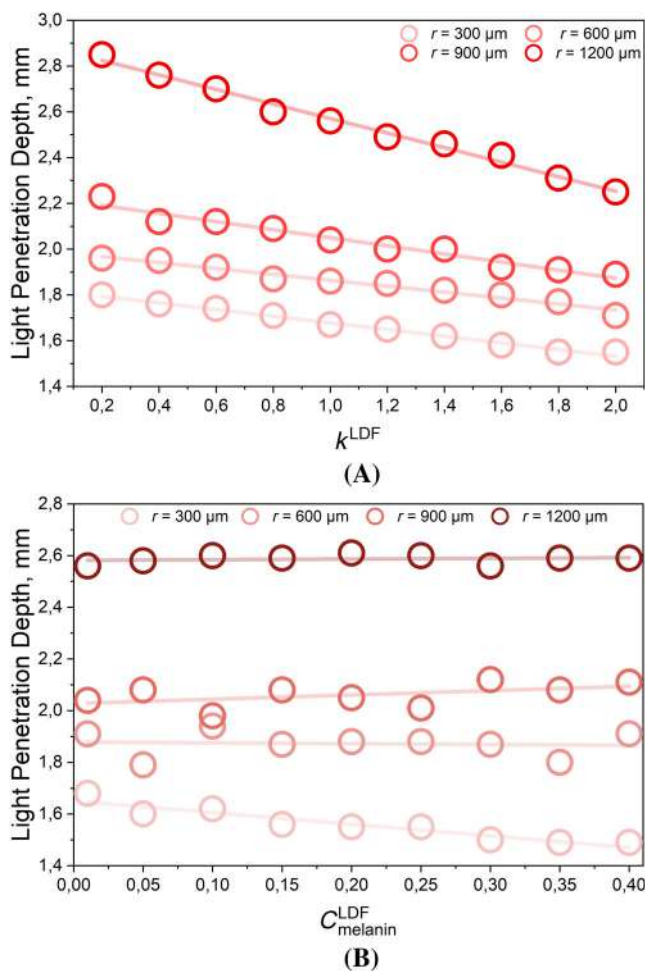
FIGURE 6 The dependence of light penetration depth in the LDF channel on (A) the tissue blood volume fraction and (B) the melanin content at different values of measurement base r. Values are presented for 10^{-3} of the incident light intensity. LDF, laser Doppler flowmetry.
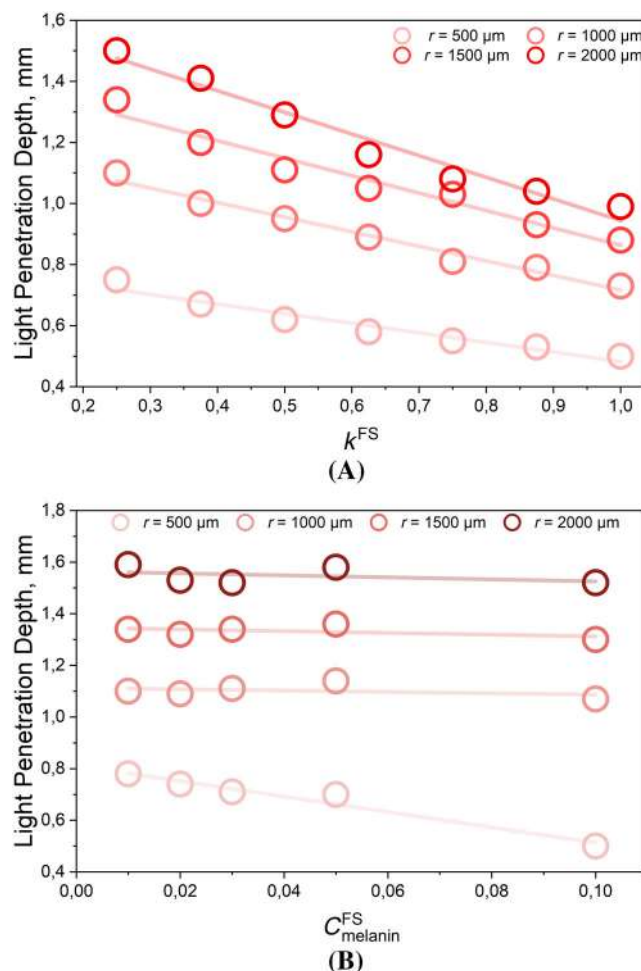
FIGURE 7 The dependence of light penetration depth in the FS channel on (A) the tissue blood volume fraction and (B) the melanin content at different values of measurement base r. Values are presented for 10^{-3} of the incident light intensity. FS, fluorescence spectroscopy.

with a variation range of r between 500 and 2000 μm. Figure 5 shows the light scattering pattern for the cases where the distance between the light source and the photodetector is 500 μm (A), 800 μm (B), and 1200 μm (C) for LDF channel and 500, 1200, and 2000 μm for FS channel.

Figure 5 shows that as the value of r increases, the depth of the penetration of optical radiation into the skin also increases, thus allowing information to be obtained from deeper vascular plexuses. For the LDF channel at $r = 500$ μm, the radiation penetration depth is the lowest and reaches about 1.5 mm, which corresponds to the upper part of the reticular dermis, and the diagnostic volume is less than 1 mm³. Increasing r up to 2000 μm increases the value of diagnostic volume up to 6–7 mm³.

For the FS channel at $r = 500$ μm, the radiation penetration depth reaches about 0.5 mm, and the diagnostic volume reaches 2–3 mm³. Increasing r up to 2000 μm

allows reaching the layer of deep blood net dermis and increases the value of diagnostic volume up to 2–3 mm³.

Furthermore, in view of the detected peculiarities of optical radiation propagation in a medium with high melanin content at large source-detector, we evaluated the combined effect of changing r and k_{LDF} and k_{FS} values as well as r and $C_{melanin}^{LDF}$ and $C_{melanin}^{FS}$. Figure 6 shows the graphical dependence of the depth of skin sensing with 850 nm light on the blood and melanin content in the tissue with different variations of the distance r. In this and the following figures, the dots indicate the data obtained, to which a linear fit has been applied (semi-transparent lines of the same color in the background) to show the linear relationship.

Figure 6 shows that for all r values, even a slight increase in skin blood flow leads to a decrease in sampling volume. However, the most significant changes occur at r equal to 1200 μm. A twofold decrease or

increase in the blood filling of the tissue in this case leads to a change in the depth of penetration of the probing radiation within 10%–12%.

In this case, the melanin content has any significant effect on the sampling volume only at r equal to 300 μm. At large values of r, most of the radiation passes directly through the epidermis into the deeper layers of the skin, thus leveling the effect of melanin. A twofold increase in $C_{\text{melanin}}^{\text{LDF}}$ at r equal to 300 μm leads to a decrease in sampling volume by 4%.

Figure 7 shows similar dependencies for the FS channel. Figure 7 shows that for all r values, increase in skin blood flow leads to a decrease in sampling volume. For the case with r equal to 2000 μm, a twofold decrease or increase in the blood filling of the tissue leads to a change in the depth of penetration of the probing radiation within 23%. The results for different variations of the $C_{\text{melanin}}^{\text{FS}}$ value are similar to the previously obtained results for the LDF channel. Only at the minimum source-detector distance ($r = 500$ μm) do changes in melanin lead to significant variations in the sampling volume.

It should also be noted that in the present work only those cases where the radiation source and receiver are located directly on the object under investigation have been simulated. Positioning the source and receiver above the skin outside direct skin contact will change the area of irradiation and the numerical aperture, which will consequently change both the light penetration depth and the sampling volume.

Thus, the results obtained showed the optimality of the used technical characteristics of wearable LDF devices, since the use of 850 nm wavelength allows receiving information from deeper vascular plexuses. In addition, deeper tissue probing is facilitated by direct tissue illumination without the use of optical fibers. This allows one to provide a larger measurement base. The obtained data confirm the dependence of the depth sensitivity of the detector on the location of the radiation source with respect to the photodetector (parameter r), which has already been noted earlier in a number of works by other authors [26, 31, 45].

Sampling volume simulation has already been performed for various designs of LDF and FS devices. Previous studies have demonstrated probing depth values in LDF channels with different wavelengths up to 0.5–0.8 mm and diagnostic volume values up to 2 mm^3 [4, 47]. Changing the design of the device, and in particular increasing the measurement base leads to a significant increase in both the depth of radiation propagation and the diagnostic volume, allowing to probe up to 1.5 mm of tissue or 8 mm^3 of its volume [48].

This is the first time that such a procedure has been applied to a wearable multimodal device that has significant differences in its technical implementation. The findings demonstrate the advantage of using wireless wearable photonic devices that directly illuminate the area under investigation without the use of optical fibers, as this allows the measurement base to be increased, resulting in a significant increase in the sampling volume. The data obtained should be taken into account when analyzing the recorded diagnostic data, and especially when comparing them with the results obtained with other technical implementations of optical diagnostic channels.

4 | CONCLUSIONS

In the present work, the simulation of optical radiation propagation in biological tissues for LDF and FS channels of a wearable multimodal diagnostic device was carried out. The sampling volume for the analyzed configuration of the wearable LDF device was studied taking into account different anatomical features of biological tissues under study. It is shown that the depth of optical radiation propagation is about 2.5 mm for the analyzed technical parameters of the device (probing wavelength 850 nm, measuring base 1200 μm, dimensions of the source and the detector of optical radiation) and the value of the diagnostic volume is about 6–7 mm^3. The obtained values meet the requirements for LDF devices as they enable examination of deep skin layers containing all segments of the blood microcirculation system.

For the FS channel the depth of optical radiation propagation reaches 1 mm for the analyzed technical parameters of the device (probing wavelength 365 nm, measuring base 2000 μm, dimensions of the source and the detector of optical radiation) and the value of the diagnostic volume is about 2–3 mm^3. One of the directions for further development of this work may be to improve the developed model, which would also allow taking into account possible age-related changes in the skin, which may influence greater or lesser depth of penetration of probing radiation into biological tissue, since it is known that skin thickness decreases linearly with ageing [49]. Differences in skin thickness between men and women are also noted [50], which should also be taken into consideration when interpreting the obtained data.

The results obtained can be used to justify specialized medical and technical requirements for wearable multimodal devices implementing LDF and FS methods. This approach will improve the reproducibility and reliability of recorded data, which will ultimately lead to an improvement in the quality of the diagnostic information obtained.

CONFLICT OF INTEREST STATEMENT

The authors declare no conflicts of interest.

ORCID

Elena V. Zharkikh https://orcid.org/0000-0001-5735-3366
Viktor V. Dremin https://orcid.org/0000-0001-6974-3505
Andrey V. Dunaev https://orcid.org/0000-0003-4431-6288

REFERENCES

[1] M. J. Leahy, J. G. Enfield, N. T. Clancy, J. O'Doherty, P. McNamara, G. E. Nilsson, *Med. Laser Appl.* **2007**, *22*, 105.

[2] A. Dunaev, *Proc. SPIE* **2022**, *12192*, 121920T.

[3] I. A. Mizeva, E. V. Potapova, E. V. Zharkikh, in *Biomedical Photonics for Diabetes Research*, CRC Press, Boca Raton, **2022**, p. 81.

[4] V. V. Dremin, E. A. Zherebtsov, V. V. Sidorov, A. I. Krupatkin, I. N. Makovik, A. I. Zherebtsova, E. V. Zharkikh, E. V. Potapova, A. V. Dunaev, A. A. Doronin, A. V. Bykov, I. E. Rafailov, K. S. Litvinova, S. G. Sokolovski, E. U. Rafailov, *J. Biomed. Optics* **2017**, *22*, 085003.

[5] A. Fedorovich, *J. Hypertens.* **2010**, *28*, e178.

[6] M. Rossi, A. Carpi, F. Galetta, F. Franzoni, G. Santoro, *Biomed. Pharmacother.* **2006**, *60*, 437.

[7] A. Rovas, I. Osiaevi, K. Buscher, J. Sackarnd, P. R. Tepasse, M. Fobker, J. Kühn, S. Braune, U. Göbel, G. Thölking, A. Gröschel, H. Pavenstädt, H. Vink, P. Kümpers, *Angiogenesis* **2021**, *24*, 145.

[8] V. V. Dremin, E. A. Zherebtsov, I. N. Makovik, I. O. Kozlov, V. V. Sidorov, A. I. Krupatkin, A. V. Dunaev, I. E. Rafailov, K. S. Litvinova, S. G. Sokolovski, E. U. Rafailov, *Proc. SPIE* **2017**, *10063*, 1006303.

[9] E. Zherebtsov, I. Kozlov, V. Dremin, A. Bykov, A. Dunaev, I. Meglinski, *IEEE Trans. Biomed. Eng.* **2022**, *70*, 3.

[10] M. J. Leahy, F. F. M. De Mul, G. E. Nilsson, R. Maniewski, *Technol. Health Care* **1999**, *7*, 143.

[11] M. J. Leahy, G. E. Nilsson, *Proc. SPIE* **2010**, *7563*, 68.

[12] J. R. Lakowicz, *Principles of Fluorescence Spectroscopy*, Springer, NY, **2006**.

[13] A. V. Dunaev, V. V. Dremin, E. A. Zherebtsov, I. E. Rafailov, K. S. Litvinova, S. G. Palmer, N. A. Stewart, S. G. Sokolovski, E. U. Rafailov, *Med. Eng. Phys.* **2015**, *37*, 574.

[14] C. L. Hu, Z. S. Lin, Y. Y. Chen, Y. H. Lin, M. L. Li, *Biomed. Eng. Lett.* **2013**, *3*, 109.

[15] W. Iwasaki, H. Nogami, S. Takeuchi, M. Furue, E. Higurashi, R. Sawada, *Sensors* **2015**, *15*, 25507.

[16] V. V. Sidorov, Y. L. Rybakov, V. M. Gukasov, G. S. Evtushenko, *Biomed. Eng.* **2022**, *55*, 379.

[17] A. V. Dunaev, *J. Biomed. Photonics Eng.* **2023**, *9*, 020201.

[18] E. A. Zherebtsov, E. V. Zharkikh, Y. I. Loktionova, A. I. Zherebtsova, V. V. Sidorov, A. I. Krupatkin, A. V. Dunaev, in *Biomedical Photonics for Diabetes Research*, CRC Press, Boca Raton, **2022**, p. 107.

[19] E. A. Zherebtsov, E. V. Zharkikh, Y. I. Loktionova, A. I. Zherebtsova, V. V. Sidorov, E. U. Rafailov, A. V. Dunaev, *IEEE Trans. Biomed. Eng.* **2023**. doi:10.1109/TBME.2023.3275654

[20] A. A. Fedorovich, Y. I. Loktionova, E. V. Zharkikh, A. Y. Gorshkov, A. I. Korolev, V. A. Dadaeva, O. M. Drapkina, E. A. Zherebtsov, *Microvasc. Res.* **2022**, *144*, 104419.

[21] M. Saha, V. Dremin, I. Rafailov, A. Dunaev, S. Sokolovski, E. Rafailov, *Biosensors* **2020**, *10*, 201.

[22] E. V. Zharkikh, Y. I. Loktionova, V. V. Sidorov, A. I. Krupatkin, G. I. Masalygina, A. V. Dunaev, *Hum. Physiol.* **2022**, *48*, 456.

[23] A. A. Fedorovich, Y. I. Loktionova, E. V. Zharkikh, M. A. Mikhailova, J. A. Popova, A. V. Suvorov, E. A. Zherebtsov, *Diagnostics* **2021**, *11*, 436.

[24] E. V. Zharkikh, Y. I. Loktionova, A. A. Fedorovich, A. Y. Gorshkov, A. V. Dunaev, *Diagnostics* **2023**, *13*, 920.

[25] A. V. Dunaev, E. V. Zharkikh, Y. I. Loktionova, A. A. Fedorovich, V. V. Sidorov, A. V. Vasin, A. A. Misurkin, V. I. Dubinin, in *Proc. 2022 Int. Conf. Laser Optics*, IEEE, NJ, **2022**, p. 20.

[26] A. V. Dunaev, E. A. Zherebtsov, D. A. Rogatkin, N. A. Stewart, S. G. Sokolovski, E. U. Rafailov, *J. Biomed. Opt.* **2013**, *18*, 107009.

[27] V. V. Tuchin, *Tissue Optics: Light Scattering Methods and Instruments for Medical Diagnostics*, 3rd ed., SPIE Press, Bellingham, WA **2015**.

[28] I. L. Shlivko, M. Y. Kirillin, E. V. Donchenko, D. O. Ellinsky, O. E. Garanina, M. S. Neznakhina, P. D. Agrba, V. A. Kamensky, *Skin Res. Technol* **2015**, *21*, 419.

[29] D. A. Rogatkin, A. V. Dunaev, L. G. Lapaeva, *Biomed. Eng.* **2010**, *44*, 66.

[30] Cloud based Monte Carlo tool for photon transport. https://www.biophotonics.fi, Accessed 2023–04–17.

[31] I. V. Meglinskii, S. J. Matcher, *Opt. Spectrosc.* **2001**, *91*, 654.

[32] A. Doronin, I. Meglinski, *Biomed. Opt. Express* **2011**, *2*, 2461.

[33] G. I. Petrov, A. Doronin, H. T. Whelan, I. Meglinski, V. V. Yakovlev, *Biomed. Opt. Express* **2012**, *3*, 2154.

[34] I. S. Saidi, S. L. Jacques, F. K. Tittel, *Appl. Opt.* **1995**, *34*, 7410.

[35] A. Roggan, K. Dorschel, O. Minet, D. Wolff, G. Muller, *Laser-Induced Interstitial Therapy*, SPIE Press, Bellingham, WA, **1995**, pp. 10–44.

[36] H. Ding, J. Q. Lu, W. A. Wooden, P. J. Kragel, X. H. Hu, *Phys. Med. Biol.* **2006**, *51*, 1479.

[37] J. Mobley, T. Vo-Dinh, V. V. Tuchin, *Biomedical Photonics Handbook*, CRC Press, Boca Raton, **2015**, p. 23.

[38] E. Salomatina, B. Jiang, J. Novak, A. N. Yaroslavsky, *J. Biomed. Opt.* **2006**, *11*, 064026.

[39] M. J. C. Van Gemert, S. L. Jacques, H. J. C. M. Sterenborg, W. M. Star, *IEEE Trans. Biomed. Eng.* **1989**, *36*, 1146.

[40] N. Bosschaart, G. J. Edelman, M. C. G. Aalders, T. G. van Leeuwen, D. J. Faber, *Lasers Med. Sci.* **2014**, *29*, 453.

[41] V. V. Dremin, A. V. Dunaev, *J. Opt. Technol.* **2016**, *83*, 43.

[42] V. Dremin, N. Golubova, E. Potapova, A. Dunaev, *J. Biomed. Photonics Eng.* **2021**, *7*, 40306.

[43] R. Hennessy, W. Goth, M. Sharma, M. K. Markey, J. W. Tunnell, *J. Biomed. Opt.* **2014**, *19*, 107002.

[44] D. Kurakina, V. Perekatova, E. Sergeeva, A. Kostyuk, I. Turchin, M. Kirillin, *Laser Phys. Lett.* **2022**, *19*, 035602.

[45] V. Dremin, E. Zherebtsov, A. Bykov, A. Popov, A. Doronin, I. Meglinski, *Appl. Opt.* **2019**, *58*, 9398.

[46] V. V. Tuchin, *Handbook of Optical Biomedical Diagnostics*, SPIE Press, Bellingham, WA **2002**.

[47] I. Fredriksson, M. Larsson, T. Strömberg, *Microvasc. Res.* **2009**, *78*, 4.

[48] E. A. Zherebtsov, A. I. Zherebtsova, A. Doronin, A. V. Dunaev, K. V. Podmasteryev, A. Bykov, I. Meglinski, *J. Biomed. Opt.* **2017**, *22*, 040502.

[49] S. A. M. Shuster, M. M. Black, E. V. A. McVitie, *Br. J. Dermatol.* **1975**, *93*, 639.

[50] T. Kono, J. Yamada, *Int. J. Thermophys.* **2019**, *40*, 1.

SUPPORTING INFORMATION

Additional supporting information can be found online in the Supporting Information section at the end of this article.